COSMIC AND SUBATOMIC PHYSICS REPORT
LUIP 9804
NOVEMBER 1998
ISRN LUNFD6/NFFK-7159-SE+19P
ISSN 0348-9329

Pion Production Excitation Functions in Proton-Nucleus Collisions from the Absolute Threshold to 500 MeV.

J. Mårtensson[1], M. Berg[1], L. Carlén[1], R. Elmér[1], A. Fokin[1], R. Ghetti[1], B. Jakobsson[1], B. Norén[1], A, Oskarsson[1], H.J. Whitlow[1], C. Ekström[2], G. Ericsson[2], J. Romanski[2], E.J. van Veldhuizen[2], L. Westerberg[2], J. Julien[3], K. Nybö[4], T.F. Thorsteinsen[4], S. Amirelmi[4], M. Guttormsen[5], G. Løvhøiden[5], V. Bellini[6], F. Palazzolo[6], M.L. Sperduto[6], C. Sutera[6], V. Avdeichikov[7,1], A. Kuznetsov[8,2], Yu. Murin[8]

(CHIC Collaboration)

[1] Department of Physics, University of Lund, Lund, Sweden
[2] The Svedberg Lab. and Dept. of Neutron Physics, University of Uppsala, Uppsala, Sweden
[3] Centre d'Etudes Nucléaires, Saclay, France
[4] Dept. of Physics, University of Bergen, Bergen, Norway
[5] Dept. of Physics, University of Oslo, Oslo, Norway
[6] INFN/LNS, University of Catania, Catania. Italy
[7] Joint Inst. for Nuclear Research, Dubna, Russia
[8] V.G. Khlopin Radium Inst., St. Petersburg, Russia

Cosmic and Subatomic Physics
University of Lund
Box 118
S-221 00 Lund, Sweden

Pion Production Excitation Functions in Proton-Nucleus Collisions from the Absolute Threshold to 500 MeV.

J. Mårtensson[1], M. Berg[1], L. Carlén[1], R. Elmér[1], A. Fokin[1], R. Ghetti[1], B. Jakobsson[1], B. Norén[1], A. Oskarsson[1], H.J. Whitlow[1], C. Ekström[2], G. Ericsson[2], J. Romanski[2], E.J. van Veldhuizen[2], L. Westerberg[2], J. Julien[3], K. Nybö[4], T.F. Thorsteinsen[4], S. Amirelmi[4], M. Guttormsen[5], G. Løvhøiden[5], V. Bellini[6], F. Palazzolo[6], M.L. Sperduto[6], C. Sutera[6], V. Avdeichikov[7,1], A. Kuznetsov[8,2], Yu. Murin[8]

(CHIC Collaboration)

[1] Department of Physics, University of Lund, Lund, Sweden

[2] The Svedberg Lab. and Dept. of Neutron Physics, University of Uppsala, Uppsala, Sweden

[3] Centre d'Etudes Nucléaires, Saclay, France

[4] Dept. of Physics, University of Bergen, Bergen, Norway

[5] Dept. of Physics, University of Oslo, Oslo, Norway

[6] INFN/LNS, University of Catania, Catania. Italy

[7] Joint Inst. for Nuclear Research, Dubna, Russia

[8] V.G. Khlopin Radium Inst., St. Petersburg, Russia

Abstract

Pion production excitation functions in proton-nucleus collisions, from below the absolute threshold to 500 MeV, has been measured with 1 MeV beam energy resolution at the CELSIUS storage ring, operating in slow ramping mode. Total yields of π^+, angular distributions and target mass dependence are presented. Comparisons with molecular dynamics calculations show very good agreement with data except very close to threshold, and for very large emission angles.

1 Introduction

The threshold energy (E_{th}) for (charged) pion production in free nucleon-nucleon(NN) collisions is 288 MeV which decreases substantially in nucleon-nucleus collisions due to Fermi motion or collective (multinucleon) interaction. A fully collective p + ^{84}Kr (pionic fusion) reaction would e.g. give $E_{th} \approx 141$ MeV. If a nucleon in the Kr nucleus is given the normal Fermi momentum one actually finds an E_{th} value for NN scattering close to the collective one even if recoil momentum and binding energy are properly introduced.

Several different models are able to reproduce the basic features of pion production at energies around the free NN threshold. To follow the changes and understand the production mechanisms deeper down in the subthreshold region more systematic experimental data than presently exist are needed. In order to improve on this, we carried out a series of experiments at the CELSIUS storage ring, with a proton beam of continuously increasing energy, from below the absolute pion production threshold up to 500 MeV, impinging on various gas-jet targets. Data were collected continuously during such beam energy cycles. This program has later on also been followed up by similar measurements in nucleus-nucleus collisions [1].

In this paper, we report on total yields, differential cross-sections, angular distributions and target mass dependence for p + N, Ar, Kr, Xe reactions. Mean-field + NN scattering (molecular dynamics, MD) calculations are introduced to compare with data.

2 The Experiment

2.1 The Celsius Storage Ring

The internal PIG source produces an H_2^+ beam with up to 10 eμA which is accelerated in the Gustaf Werner Cyclotron (GWC), up to 98 MeV and then transported to the CELSIUS storage ring [2] where it is introduced by stripping injection. About 1x10^{11} protons are typically stored in the CELSIUS ring. When injecting heavy ion beams also multiturn injection is used. These beams can be accelerated up to energies of 1.36 GeV (protons) or 470A MeV (Z/A = 1/2 ions). Electron cooling for beams with velocities corresponding to an electron energy of 300 keV is possible. Cooling during the slow ramping is however extremely difficult and is not used in the experiments discussed in this paper.

A cluster gas-jet target [3] produces gas streams between the cooled nozzles with a thickness of up to $1 \cdot 10^{14}$ atoms/cm^2 for light gases (N, Ne) and $2 \cdot 10^{13}$atoms/cm^2 for the heavy ones (Xe). These fluxes give typical half-lifes of the proton beam from one to five minutes. The life-time depends rather strongly on the beam energy. After the

injection phase, the beam is accelerated during 22 s to the start energy for data taking. At this moment the gas jet is switched on, and the beam energy is continuously increased by slow ramping of the magnets. In the very first experiment of this kind [1], we utilized two (overlapping) ramp cycles covering beam energies of 170-270 MeV and 250-500 MeV. In the second experiment, we used only one wider ramp covering 150-500 MeV. A typical ramp cycle lasts for 250 s, then the gas-jet is switched off, the beam is dumped and a new cycle starts with proton injection (Fig. 1). The cycles, chosen in our experiments, were 300 s long, except for the low energy cycles with Kr and Xe targets, where 120 s cycles were used due to the shorter lifetime. It was always required that at least 1/3 of the stored protons should remain at the end of the cycle.

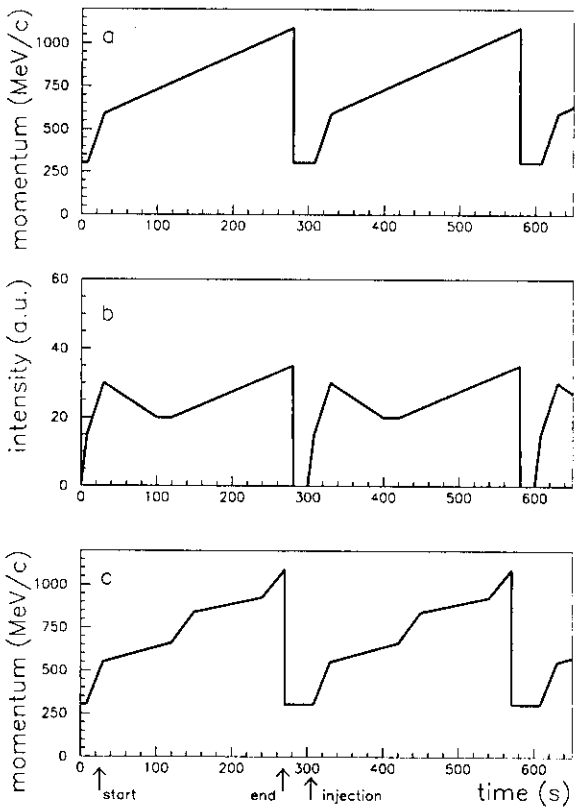

Fig. 1: Principle sketch of a) the beam momentum cycle, b)the beam intensity variation and c) the beam momentum ramp utilized in the second experiment.

The luminosity, $L = \nu \cdot \phi \cdot t \cdot f$, varied between 10^{30} and 10^{31} cm^{-2} s^{-1}. Here ν is the frequency, ϕ is the number of stored protons, t is the target thickness and f accounts for the effective gas-jet/beam overlap. The beam energy in each event is obtained by starting a clock in the data aquisition (DAQ) at t = t_{start} (see Fig. 1) and the time is then read out when an event trigger is obtained. The event time (t_{event})

is translated to beam energy by the frequency-time table registered continuously in the accelerator control. This gives the individual collision energy from the frequency as,

$$E_{event} = (\frac{1}{\sqrt{1-\beta^2}} - 1) \cdot M \tag{1}$$

where $\beta = \nu \cdot 81.8$ /c.

The high precision in the frequency determination and the extremely good reproducability of the ramping cycle make the precision in the event energy determination quite high, $\Delta p/p \sim 1.5 \times 10^{-3}$. In our first experiment we used a linear p_{beam}-time relation in the ramp whereas in the second experiment we operated with three different dp/dt gradients in order to assure collection of large enough statistics in regions of special interest (Fig. 1c). These regions are the absolute threshold region and the region where narrow resonances in the pion production have been reported. Actually it turned out that almost any forms of ramp cycles can be created and reproduced with high precision at CELSIUS.

2.2 The Range Telescopes

Five plastic scintillator (NE102) pion sandwich range telescopes were used to detect charged pions [4]. The telescopes were placed at 20°, 55°, 75°, 97° and 120° in the first experiment and in the second experiment at 20°, 55°, 75°, 90° and 150°. Each telescope consists of ten detectors, the last one operating in veto mode. The individual detector thicknesses are chosen to give approximately equal energy bins Coincident signals from the first three detectors form the trigger. Thus we include in the data pions that stop in detectors 3-9 which, according to thicknesses and range-energy tables, correspond to energy intervals of 11 - 60 MeV in the 20^o telescope, 11 - 84 MeV in the 55^o and 75^o telescopes and 16 - 75 MeV (exp. 1) or 15 - 75 MeV (exp. 2) in the 97 or 90^o and backward telescopes. The first three detectors were separated by several cm in order to get good enough directional sensitivity to avoid background from particles not produced in the beam-target overlap volume. Philips XP 2020 PM-tubes were used to read out all detectors except those in the forward telescope, where the limited space required 3/4" tubes (Hamamatsu R1166). This type of range telescopes has proven earlier to be a powerful instrument for subthreshold charged pion studies, especially for π^+ [4, 5, 6]. The main advantages for subthreshold measurements are:

- Fast signals allow operation at high countrates.
- Good discrimination of π^+ vs. π^- and very good discrimination against other singly charged particles.
- Provision of a powerful hardware trigger for pions.

2.3 Electronics

The pion trigger requires a coincidence between the first three detectors in a telescope, when each of these produces a signal above a discriminator level of ~30mV. The coincidence overlap time for this trigger was set to 30 ns. All signals in detectors 1 to 7 are also compared to a second, high discriminator threshold. A veto is created if any signal in detectors 1, ..., S-2 (S stands for stop detector) lies above this level. This gives a hardware rejection against protons and heavier particles. Due to this powerful proton rejection, the data collection could be performed at a rate nearly matching the maximum luminosity. The whole logic chain is produced in about 100 ns and the analog signals for the ADCs have to be delayed by the same amount of time in order to have the gate signal arriving 10 ns before them. If the particle has not been rejected at this stage, a trigger is sent to open the ADC gates, unless the CAMAC readout system is busy and vetoes the new event. The detector where the pion comes to rest (the stop detector) is determined by a pattern unit which registers one bit for each detector having a signal which exceeds the 30 mV discriminator level.

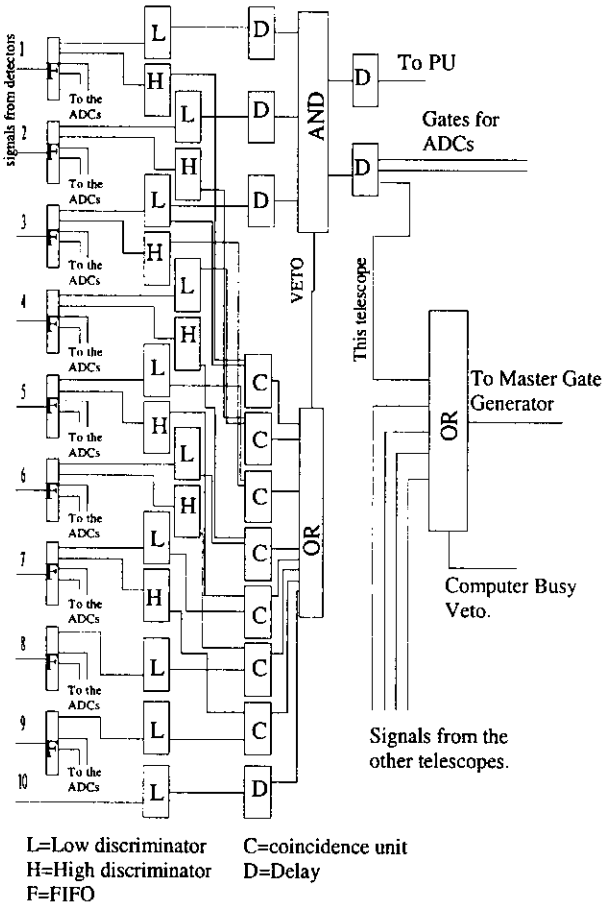

Fig. 2: Block scheme for electronics

2.4 Pion Identification

In order to separate π^+ from π^- each analogue signal is integrated in two different ADC:s with individually adjusted gates (see Fig. 2). The first gate is ~100 ns long and opens the ADC ~10 ns before the maximum of the analog pulse appears. The rise-time of the signal is 6-7 ns and the second gate, ~90 ns long, opens another ADC a few ns after the maximum. For every event trigger these two ADC values and the event time are stored by the (VME) DAQ system. This allows a separation between π^+ and π^- when plotting the prompt signal versus the delayed signal due to the fact that the latter will include also the 4.2 MeV muon signal coming from the $\pi^+ \rightarrow \mu^+\nu$ decay with a lifetime of 26 ns. The π^- is always promptly absorbed by a nucleus in the detector material at the stopping point and therefore delivers no extra muon contribution to the delayed signal. However the π^- absorption creates the problem that charged decay products from the excited scintillator (C)nucleus will add their signals to the total integrated E signal. Because of this, it is not possible to use the ΔE - E correlation to identify charged pions. Instead, all charged pions, i.e. the sum of π^+ and π^-, are identified from the ΔE signals in the 1, ..., S-1 detectors (Fig. 3a). In Fig. 3b we show a typical ΔE - E correlation plot after protons have been removed and in Fig. 3d only π^+ separated from π^- by the delayed μ^+ signal. Fig. 3c shows the separation between π^+ and π^- (+ remaining protons) in the prompt - delay signal representation. A pion which stops in detector plane 3 will have only one ΔE - ΔE correlation for its identification whereas a pion that stops in detector plane 9 has seven possible S-i-1/S-i correlations to introduce.

2.5 Normalization and Statistical and Systematic Errors

2.5.1 Normalization

In the experiments presented here, it was necessary to perform absolute normalization by a particle monitor since the absolute momentaneous luminosity, depending on both beam intensity, target gas-jet flow and the overlap between beam and target, could not be measured directly. The number of stored ions is decreasing during the cycle, due to losses both in the target and in rest-gas, but as the frequency increases during acceleration the current may still increase (see Fig. 1b). High energy (52-161 MeV) protons emitted at 97° (90° in the second experiment) were used for normalization [1]. The cross-sections for these monitor protons were calculated by a standard BUU code [7] and afterwards "absolute normalized" from empirical data [8, 9]. Since on-line proton rejection, (see section 2.3.) was introduced in all pion telescopes in the first experiment, we performed in this case also calibration runs to control the proton rejection efficiency. This was done by setting up two identical telescopes at the same angle, 97°, where one was the ordinary monitor/pion telescope and the other one was an identical telescope with proton rejection removed. In the second experiment a prescaler allowed 1/16 of the events to be registered without proton rejection. The

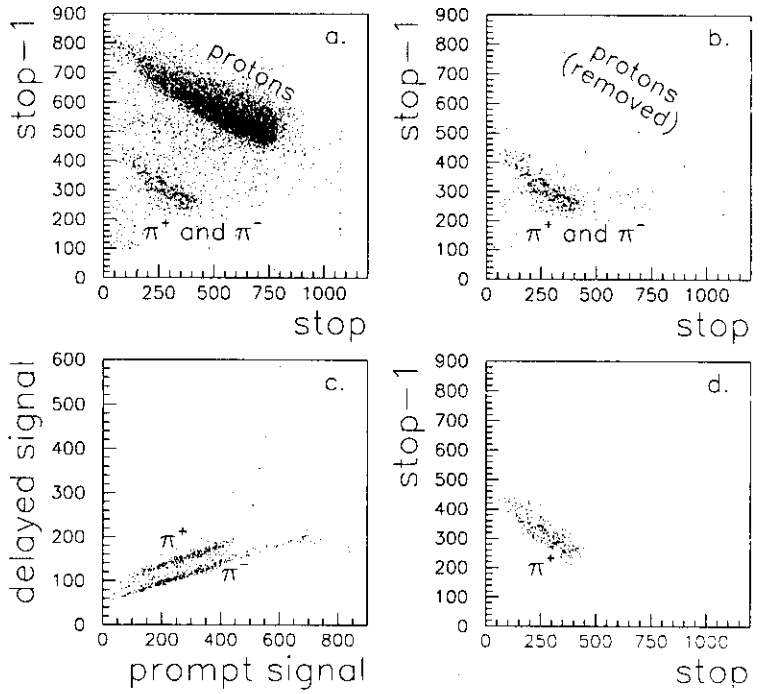

Fig. 3: a) ΔE - E correlation of π^+ and π^-. The protons have been removed by the regular cuts in the ΔE-ΔE correlations. b) ΔE - E correlation of π^+. c) Plot of a typical prompt signal-delayed signal correlation.

pion cross-sections are thus given in the first experiment by,

$$\frac{d\sigma_\pi}{d\Omega} = f_{eff} \cdot \frac{N_\pi}{N_p} \cdot \Delta\Omega \cdot \left(\frac{N^c_{\pi nr}}{N^c_{\pi r}} \frac{N^c_{pr}}{N^c_{pnr}}\right) \cdot \int_{52}^{161} \frac{d^2\sigma_p}{d\Omega dE} dE. \tag{2}$$

and in the second experiment by a simpler formula,

$$\frac{d\sigma_\pi}{d\Omega} = f_{eff} \cdot \frac{N_\pi}{N_p} \cdot \Delta\Omega \cdot \frac{1}{16} \cdot \int_{52}^{161} \frac{d^2\sigma_p}{d\Omega dE} dE. \tag{3}$$

f_{eff} is here an efficiency factor which corrects for pion decay in flight - also during slow down in the detector material, for pion-nucleus collisions in the detector material and for π^+ it also accounts for the inefficiency in the prompt/delay ADC signal identification method [11]. $\Delta\Omega$ is the solid angle correction for eventual differences between the monitor telescope and the telescope in which the pions were registered. N_π/N_p is the registered pion to proton ratio which is corrected either from the special normalization run (denoted c) through the expression within brackets in (2) (r stands for rejected and nr for non-rejected particles) or through the prescaling factor 1/16

in (3). The integral is the proton cross-section for the monitor telescope, determined as described above.

2.5.2 Systematic Errors

Based on comparisons between overlapping data taken both with low- and high energy ramps in the first experiment and on comparisons between p + Kr data from the first experiment and the second, single ramp experiment, we estimate the uncertainty in the determined N_π/N_p ratio to be at most 20%. The latter comparison is exploited in Fig. 4. Other systematic errors, mainly coming from the correction factors, are similar for the two experiments. Computer dead-time and luminosity variations do not contribute due to the fact that we use ratios between yields of two kinds of particles, registered under identical conditions. The loss of π^+ in the analysis is connected to the resolution in the delayed-prompt method which depends on how well the gate setting is made for the pulse shape analysis. Delaying the start of the second gate improves the resolution but then the π^+ efficiency decreases because of the increasing number of pions that decay before the delayed gate is opened.

The efficiency of the muon registration has been measured directly for the backward $(97°, 120°)$ telescopes [11] to be 90% while it is determined by Monte Carlo calculations for the 55° and 75° telescopes to be 82% and for the 20° telescope to 77%. The differences come essentially from the different geometries of the telescopes. The corrections for decay-in-flight, geometry and scattering, gives a total systematic uncertainty of 15%. A systematic error of 4% is introduced for the determination of the solid angles of the different detectors. The BUU calculations for the proton cross section introduce a systematic error of 20%, and in the first experiment, an additional 12% systematic error is estimated for the additional efficiency calibration of the proton monitor. The efficiency in the pion selection process of the data analysis contributes with 4% to the systematic error.

When integrating up the total yield, we extrapolate the pion energy distribution, outside the range of the telescopes. These extrapolations were determined by the normalized BUU calculations which were also used to interpolate between the measured angles in order to perform angular integration. The uncertainties in these estimations contribute with 20% to the systematic error.

All systematic uncertainties add up to a total error of 35%, except for the lowest beam energies, very close to the absolute pion production threshold, where the total error is $\sim$ 50%, mainly because of an increasing uncertainty in the estimated proton cross sections and in the determination of the flat general background which is important only here (see Fig. 4). The estimation of the systematic errors seems well confirmed by comparisons to earlier data from fixed-target experiments (see next chapter).

2.5.3 Statistical Errors

The statistical errors have contributions from both pions and protons since the ratio between the yields of these particles are introduced. The contribution from protons is however nearly negligible. The statistical errors are presented in the figures normally bars only for a few points as typical examples. The statistical fluctuations are however easy to recognize in the excitation function figures.

3 Experimental Results

3.1 π^+-production

In Table 1. we present the data samples to be discussed in this section. The differences between experiments 1 and 2 are explained in the previous chapter. We stress that data in exp. 1 were collected in two parts with a low beam energy ramp, 169 - 270 MeV and a high energy ramp, 250 - 500 MeV, while exp. 2 contained only one single ramp with energies 150 - 500 MeV.

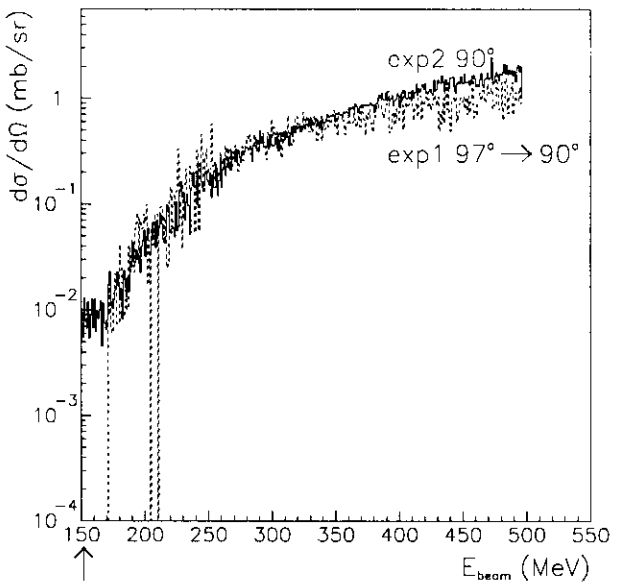

Fig. 4: Comparison between 90°, π^+ cross-sections in p + Kr collisions measured in experiments 1 and 2. The arrow denotes the absolute threshold.

In Fig. 4, a comparison is made between the absolute differential cross sections, $d\sigma/d\Omega$, of 16 - 75 MeV π^+ emission at 90° measured in the two p + Kr experiments, after the (very small) 97° $\rightarrow$ 90° extrapolation of the exp. 1 data has been made. The 55° and 75° data are obtained at exactly the same angles in the two experiments but since the statistics in these cases are smaller we judge the 90°/97° data to be

Reaction	Angular position	Beam energy	Comment
p + N	55^o, 75^o, 97^o, 120^o	169 - 500 MeV	exp. 1
p + Ar	55^o, 75^o, 97^o, 120^o	169 - 500 MeV	exp. 1
p + Kr	55^o, 75^o, 97^o, 120^o	169 - 500 MeV	exp. 1
p + Kr	20^o, 55^o, 75^o, 90^o, 150^o	150 - 500 MeV	exp. 2
p + Xe	55^o, 75^o, 97^o, 120^o	169 - 500 MeV	exp. 1

Table 1: List of data sets

most relevant for a normalizing comparison. The beam energy dependence is slightly stronger in the new data than in the old high energy ramp data whereas the comparison with the low energy ramp data shows no differences. The 55° and 75° data do show the same tendencies. The differences do fall within the systematic errors, presented in [1] and in section 2.5.2 above. Since the most plausible explanation for the difference at high beam energies is related to the difference in the normalizing procedure, which is simpler and more reliable in the latest experiment, all data in the first experiment have subsequently been corrected by the energy dependent ratio (R_{12}) between the cross sections from exp. 2 and exp. 1.

The data in Fig. 4 have not been corrected for eventual remaining background that fulfil all conditions on the ADC signals. The experimental beam energy cutoff is at 169 MeV in the old data and at 150 MeV in the new data. The new data which extend even below the threshold for producing a 16 MeV pion at 90° (see arrow in Fig. 4), confirm that there is a background with no observable beam energy dependence. This background, which is negligible for energies >200 MeV and only important very close to the absolute threshold, has been removed in all subsequent figures.

Figure 5 shows the total yield of π^+ in p + ^{14}N and p + ^{40}Ar reactions compared to earlier data [10] for reactions as close as possible to those measured in this experiment. The yields have been extrapolated below the experimental low-energy cutoff for pions and above the high-energy cutoff by using predictions from a standard BUU code [7] normalized in the measured pion energy region [1]. The angular dependence has been obtained from a polynomial fit, $d\sigma/d\Omega = a\cdot\cos^2\Theta + b\cdot\cos\Theta + c$, to the five (or for p + Kr seven) data points available. The comparisons in Fig. 5 show good agreement, except possibly in the deep subthreshold region where up to a factor of two larger yields are measured in our experiment. It should be stressed that the target mass dependence should be responsible for $\sim$ 20% lower p + C than p + N yield in the deep subthreshold region and $\sim$ 10% in the high energy region. The systematic errors in our experiments, estimated in the previous chapter, are largest for the lowest beam energies where it can be up to 50% and in the conventional (spectrometer) experiments, normally systematic errors of the order of 30% are reported. The statistical errors are furthermore of the order of 20% for the low energy points in the spectrometer experiments. The overall agreement is therefore acceptable and within the estimated experimental errors.

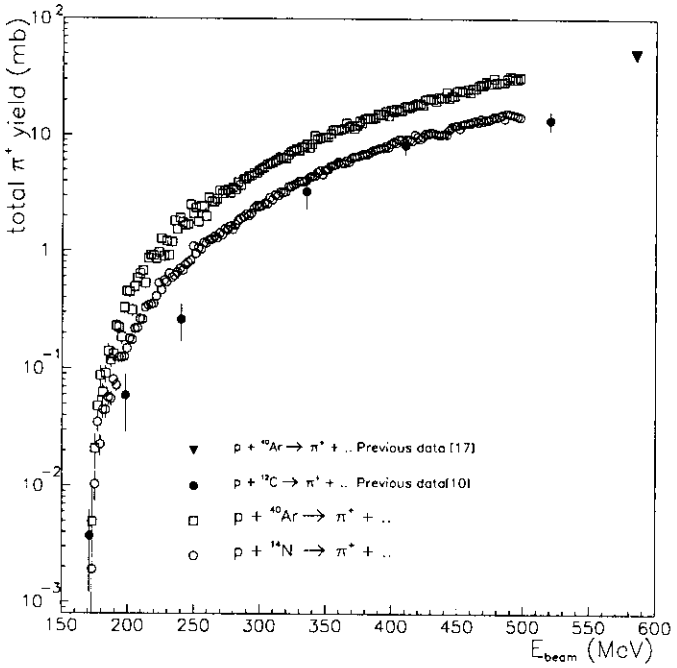

Fig. 5: The total yield of π^+ in p + N and p + Ar collisions compared to earlier results.

Well established microscopic- as well as mean-field+NN models have been developed to describe the full dynamical evolution and the particle emission in both p - nucleus and nucleus - nucleus collisions. The Dubna cascade model [14] produces pions both in direct NN scattering and in two-step reactions with an intermediate Δ or off-shell nucleon. Absorption and rescattering affect the original pion spectra here as well as in any proper model. The good agreement between our p + Ar data and these calculations have been presented in ref. [19]. The BUU model [7] is the classical representative of the second kind of models in which the dynamical evolution is prescribed through equations that contain both interaction with the mean field and between individual nucleons (actually each nucleon is made up of a number of test particles). We have shown in [1] that this model generally overpredicts the pion yield, particularly the backward yield. Explanations for this mis-match have been suggested to come from the omission of the direct pion production channel and from the fact that no local, momentum dependent interaction potential has been introduced.

In this paper we chose instead to compare data with calculations from a molecular dynamics model [18] where direct pion production in nucleon-nucleon collisions is introduced. In this model the mean field dynamics are based on the nucleon molecular dynamics model described in [12]. The nucleons are represented by Gaussian wave packets moving in a self-consistent mean field according to classical (Ehrenfest) equations of motion. The Hamiltonian of the interacting system is written as,

$$H = \sum_{i=1}^{A} \frac{\vec{p}_i^2}{2m} + \frac{1}{2}\sum_{i=1}^{A} V_{Skyrme}(\vec{r}_i) + \frac{1}{2}\sum_{i=1}^{Z}\sum_{k=1,i\neq k}^{Z} \frac{e_1 e_2}{|\vec{r}_i - \vec{r}_k|} \tag{4}$$

where the "soft" equation of state in the Skyrme representation

$$V_{Skyrme}(\vec{r}_i) = -356\left(\frac{\rho(\vec{r}_i)}{\rho_0}\right) + 303\left(\frac{\rho(\vec{r}_i)}{\rho_0}\right)^{7/6} \tag{5}$$

was chosen. The momentum vector of the pion is chosen stochastically. Introduction of the Pauli principle, which prevents scattering into already occupied regions of phase-space, are incorporated into the model. Pions are produced in direct nucleon-nucleon collisions, propagate in the Coulomb+nuclear potential of the surrounding nuclear matter and can be reabsorbed (rescattered) in inverse πNN reactions. The pion reabsorption is based on the energy dependent pion mean free path given by the optical model [16].

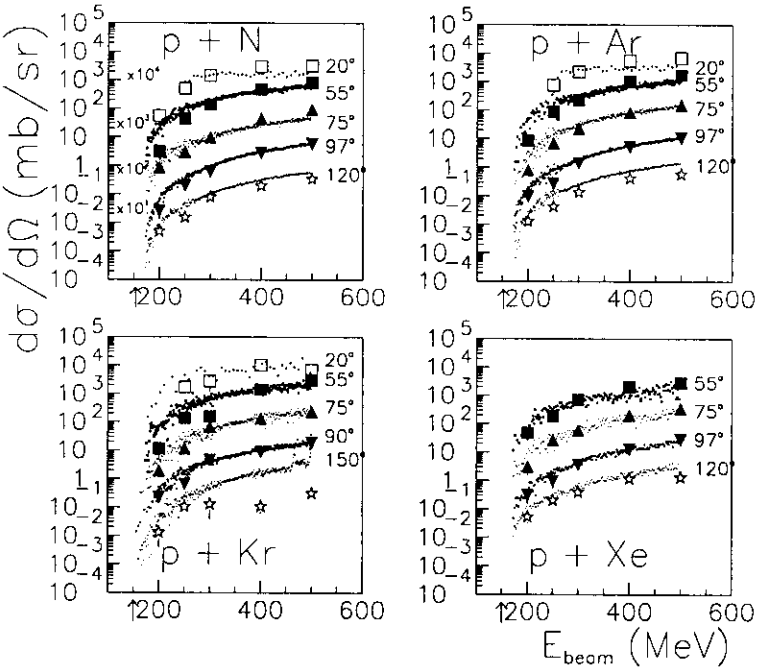

Fig. 6: The beam energy dependence of differential $\frac{d\sigma}{d\Omega}$ cross-sections in p + N, p + Ar, p + Kr, and p + Xe reactions. All absolute levels in the figure are multiplied by factors of ten as denoted in the p+N figure. All large points represent cross sections from MD calculations. The arrows show the absolute the absolute threshold for 0° emission. The energy integration is explained in the text.

Fig. 6 presents the beam energy dependence of all differential cross sections, measured with high enough statistics. The substantially larger statistics in the beam energy region 300 - 400 MeV in the p + Kr data reflect the demands from the search of narrow resonances to be reported elsewhere. All data cannot be directly compared

since they are integrated over pion energy in the region 16 - 75 MeV, for the 90°, 120° and 150° telescopes whereas the 55° and 75° telescopes are integrated over 11-83 MeV and the 20° telescope over 11-60 MeV . The arrows indicate the absolute threshold for the fully collective reaction p + X $\rightarrow \pi^+(E_\pi > E_\pi^{min} + \cdots)$.

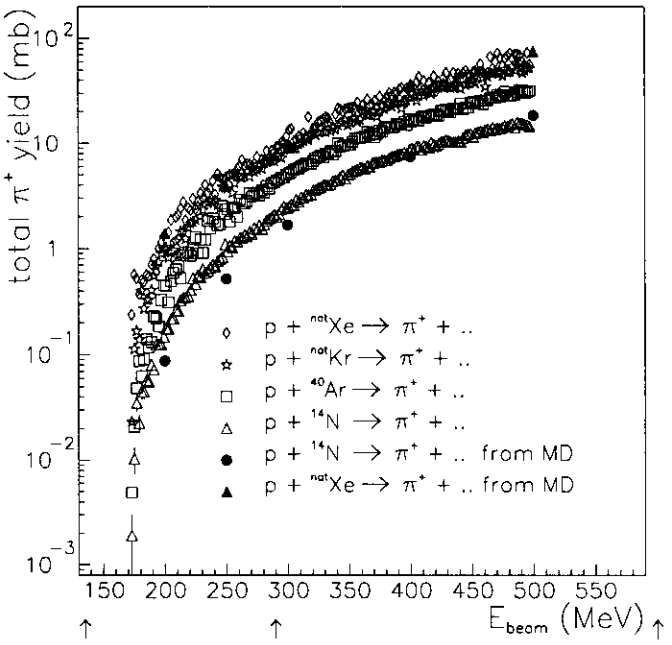

Fig. 7: The beam energy dependence of the total yield of π^+ in p + N, p + Ar, p + Kr, and p + Xe reactions. The left arrow shows the absolute threshold (for p+Kr), the second arrow the free NN threshold and the third arrow the corresponding 2π threshold.

Fig. 7 shows the total integrated cross sections for all four reactions. In this case extrapolations of cross sections below and above the detection region are performed in the way described in section 3.1 and therefore all data are directly comparable. In all reactions a smooth increase is found with increasing beam energy, without any drastic discontinuities. The increase is very steep close to the absolute threshold (left arrow), but then it levels off around the free NN threshold. The leveling off stops however and the slope remains constant up to 500 MeV. When comparing the data to MD calculations it appears as if this model describes the general tendency of the beam energy dependence quite well except at the very lowest energies where introduction of collective phenomena become important. It also appears from the 150° p+Kr data (Fig. 6), as if the MD calculations underestimate backward production of pions rather severely. This could either be due to the isotropic choice of the NN $\rightarrow$ NN+π angular distribution or to the way reabsorption is treated.

3.2 Target Mass Dependence

The target mass dependence of the total yield of π^+ is stronger in the light mass region. This has been observed earlier and follows also the tendency in nucleus-nucleus reactions [4]. This fact is further exploited in Fig. 8, where the exponent, τ, in the assumed power law dependence, $\sigma \sim A^\tau$, is determined by using the ratios of all six available target pair combinations.

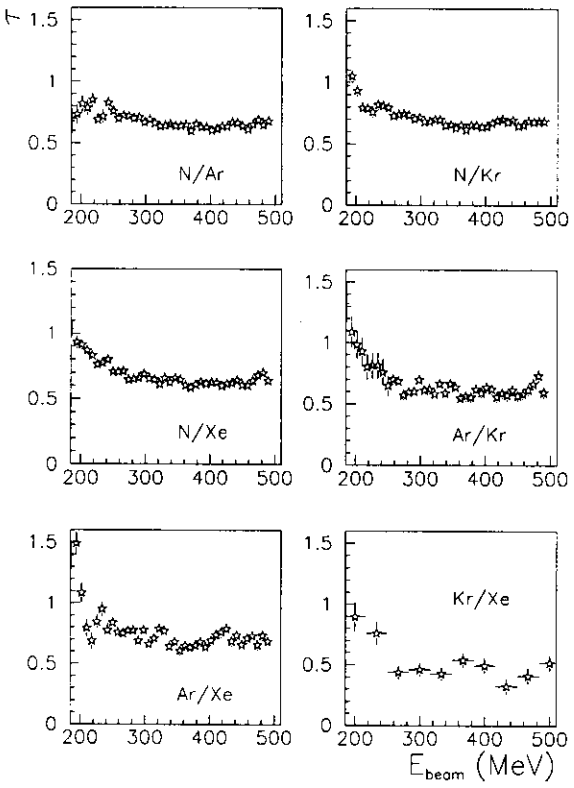

Fig. 8: The beam energy dependence of the exponent τ (see text) from the ratio of the yield of π^+.

Actually, τ is larger than unity for the very lowest beam energies (not explored in Fig. 8) because the difference in absolute threshold in reactions with different targets is important there. Apart from this, it appears as if τ proceeds from unity close to the threshold, indicating a strong collective (volume-) effect in the pion production mechanism, to an asymptotic level varying between 1/2 for the heaviest target nuclei to 2/3 or even more for light target nuclei (Table 2).

This may indicate that the black disc scattering picture is relevant for light targets but that it turns into a surface-like scattering or alternatively that reabsorption of pions, which becomes increasingly important with the target, is responsible for this.

Cross sec. ratio	τ_{asympt}	τ_{250}	τ_{200}
N/Ar	0.68±0.05	0.70±0.08	0.80±0.09
N/Kr	0.70±0.05	0.83±0.08	0.97±0.09
N/Xe	0.62±0.05	0.74±0.07	0.95±0.07
Ar/Kr	0.61±0.06	0.73±0.07	1.08±0.07
Ar/Xe	0.70±0.07	0.90±0.08	1.1±0.1
Kr/Xe	0.40±0.1	0.60±0.15	0.95±0.20

Table 2: The exponent τ, $\sigma \sim A^{\tau}$, for the target mass dependence. The index τ stands for the beam energy of the power law fit. .

The general E_{beam} dependence may in other words indicate that a strong collective prescription or a first chance NN collision model, with short enough mean-free-path for pions, gradually must be replaced by either mean-field prescriptions [13] or alternatively by complete NN scattering models of cascade type [14, 15].

3.3 Angular Distributions

The proper inertial system in which the angular distributions of pions from p + nucleus collisions should be presented ranges from the (total) c.m. system to the NN (mean speed) system. The limited (lab. system) energy region for pion measurements and the finite number of measured lab. angles make however, such transformations of limited value. This also makes invariant cross section contour plots in the $p_{\|}$ - $p_{\perp}$ or $v_{\|}$ - $v_{\perp}$ space of little use. Therefore we chose to present only standard $d\sigma/d\Omega$ differential cross section as a function of Θ_{lab} (Fig. 9) for various beam energies. It should be stressed that in all cases the pion energy intervall is 15-75 MeV after introduction of some extraction for the 20° points (see section 3.1).

The following general conclusions can be drawn:

i) The forward peaking of the pion emission at lower beam energies shifts to more symmetric or in some cases even backward peaking at high beam energies.
ii) The backward emission shows a stronger beam energy dependence than the forward emission.
iii) The forward/backward emission shows a distinct dependence on the target mass.

These observations do confirm a decreasing importance of the individual NN scattering process with decreasing beam energy. They also stress the importance of a proper treatment of pion reabsorption [20]. The MD calculations (not exploited here), following the prescription in section 3.1, reproduce the data well with the two exceptions already noticed in section 3.1, the emission is underestimated at 180 MeV as expected close to the absolute threshold, and also the 150° emission in p+Kr is underestimated.

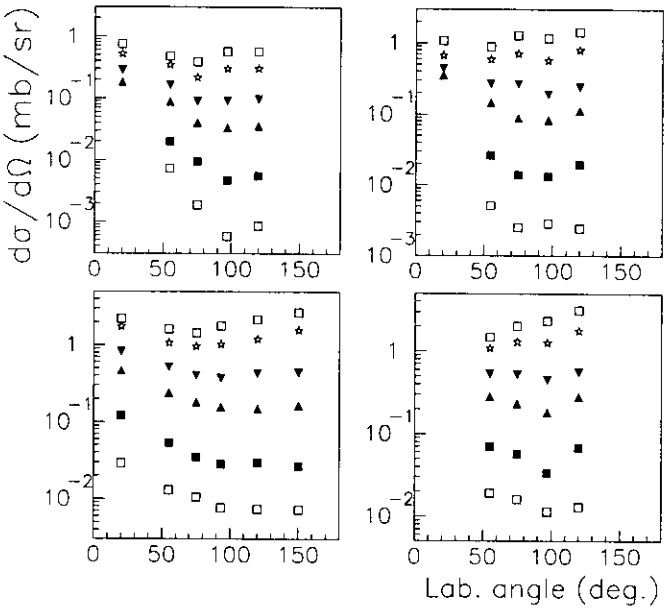

Fig. 9: $d\sigma/d\Omega$ for 15-75 MeV π^+ in p + N, p + Ar, p + Kr, and p + Xe reactions. The beam energies are from bottom to top: 180, 200, 250, 300, 400, and 500 MeV.

4 Conclusions

Excitation function data on π^+ production in p - nucleus collisions from the absolute threshold to 500 MeV, i.e. to the Δ dominated region, have been presented. The method of taking data continuously during a slow ramping cycle of a stored beam that interacts with an ultra-thin gas-jet target is confirmed by comparisons to other data and by comparisons between data from two different experiments.

The target mass dependence evolves from $\sim A^1$ to $\sim A^{2/3}$ or even $\sim A^{1/2}$ for heavy targets when going from threshold beam energies to higher energies, indicating the decreasing importance of processes that involves the whole volume of the system. However, also for more surface-like reactions where individual NN scattering dominates reabsorption is important which partly explains the decreasing A dependence with increasing target mass.

The angular distribution proceeds from symmetric or even backward scattering for the highest beam energies to clear forward peaking at threshold (as expected).

The beam energy dependence of the cross sections are reasonably well described by mean-field + NN scattering calculations except for an underestimation at very large angles and a general underestimation at the lowest energies very close to the absolute threshold where collective processes play an important role.

Acknowledgements

The authors thank the accelerator staff of The Svedberg Laboratory for its excellent technical support and the Swedish Natural Science Research Council for its financial support.

References

[1] B. Jakobsson et al., Phys. Rev. Lett. 78, 3828 (1997).

[2] T. Bergmark et al., TSL Progress Report 1987-1991, p19 and 1992-1993, p14 and L-O Andersson et al. TSL Progress Report 1994-1995, p12. Editor A. Ingemarsson.

[3] C. Ekström, Proc. 19th Int. Symp. on Cooler Rings and their Applications, Tokyo, p228. Word Sci.Publ. Company. Editors T. Katayama and A. Noda.

[4] B. Norén et al., Nucl. Phys. A489, 763 (1988).

[5] T. Johansson et al., Phys. Rev. Lett. 48, 732 (1982).

[6] V. Bernard et al., Nucl. Phys. A423, 511 (1984).

[7] B. Li and W. Bauer, Phys. Rev. C44, 606 (1991).

[8] W.A. Richter et al., Phys. Rev. C49, 1001 (1994).

[9] A.A. Cowley et al., Phys. Rev. C43, 678 (1991).

[10] B. Million (private communication); B. Jakobsson, Phys. Scr.48, 179 (1993)

[11] G. Sanouillet et al., CEN Saclay Internal Report CEA-N-248 (1986).

[12] J.P. Bondorf, D. Idier andI. Mishushtin, Phys. Lett. B359 261 (1995).

[13] W. Cassing, V. Metag, U. Mosel and K. Niita, Phys. Rep. 188, 363 (1988).

[14] K.K. Gudima, H. Iwe and V.D. Toneev, J. Phys. G5 229 (1979).

[15] J. Cugnon, T. Mizutani and J. Vandermeulen, Nucl. Phys. A532, 505 (1981).

[16] P. Hecking, Phys. Lett. 103 B, 401 (1981)

[17] J.F. Crawford et al., Phys. Rev. C22 1184 (1980)

[18] A. Fokin Licentiate Thesis, Faculty of Science, Lund University 1997

[19] K. Gudima, M. Ploszajcak, GANIL Preprint 98 17

[20] G. Ericsson, B. Jakobsson, Proceedings of the First European Biennial Workshop on Nuclear Physics, Megève, France, 1991, p. 200, ed. by D. Guinet and J.R. Pizzi.